Comparison of an Electron−Atom-Scattering Description with Gas-Phase Scattering Data for He, Ne, Ar, Kr, and Xe

Douglas G. Frank* and Arthur T. Hubbard*

Surface Center and Department of Chemistry, University of Cincinnati, Cincinnati, Ohio 45221-0172

Received: May 16, 1996; In Final Form: August 29, 1996[⊗]

Recent measurements of complete Auger electron emission angular distributions from solid surfaces have pointed to the need for an accurate description of Auger electron scattering at surfaces and the angular intensity distributions which result. Presented here is a description of electron−atom scattering which includes the effects of inhomogeneous elastic scattering as required for analysis of Auger electron emission angular distributions from ordered solid surfaces. As a first test of the description, use is made of elastic scattering differential cross-section measurements reported by various workers for scattering of electrons by rare gas atoms (He, Ne, Ar, Kr, and Xe). These gas-phase data allow the elastic portion of the description to be tested in the absence of complications due to long-range structure and multiple scattering. The resulting simulations, which span the kinetic energy range from 50 to 100 eV, are found to be in good agreement with the gas-phase scattering data, suggesting future applicability to solid surfaces.

Introduction

Measurements have been reported recently of complete Auger electron angular distributions from well-characterized single-crystal surfaces, monoatomic layers, and bilayers.[1−13] Studies of monoatomic layers indicate that intensity minima are present along the internuclear directions.[9−11,14−18] Measured angular distributions for single-crystal samples at low kinetic energy (KE < 100 eV) also display intensity minima along directions corresponding to the internuclear axes.[1−13] Previous work has also revealed that a single atomic layer of iodine atoms substantially and anisotropically attenuates the Auger intensity emitted at 355 eV from an underlying silver monoatomic layer, producing a distinct attenuation pattern in which the intensity minima correspond to the internuclear directions.[13] Such data show promise for the investigation of surface structure and electron−atom-scattering phenomena. However, in order to utilize such data, it is necessary to have a theoretical description which quantitatively relates electron−atom-scattering data to surface structure and composition.

Gas-phase electron-scattering data, such as definitive results which have been reported for the rare gases (He, Ne, Ar, Kr, and Xe), are important to the development of an accurate description of Auger electron scattering in the solid state because such data allow the scattering behavior which results from single electron−atom interactions to be examined. Particularly useful are the measured values of the elastic differential scattering cross sections (intensity distribution vs scattering angle)[19−44] and the total cross sections:[45−49] *Scattering cross sections are more easily obtained from low pressure gas-phase data than from solid state data because gas-phase measurements are relatively uncomplicated by multiple scattering*. Also, structure considerations are negligible for gaseous samples, such that cross section measurements allow the relative probabilities of elastic and inelastic scattering processes to be evaluated, leading to a quantitative description which conserves electrons: For example, gas-phase scattering data for Xe show that inelastic scattering processes contribute about 72% of the total scattering cross section at KE = 350 eV[45−49] while diffuse elastic scattering and diffraction processes account for the remaining 28%.

In the present work, we offer a new phenomenological description of electron−atom-scattering behavior which is consistent with gas-phase experimental data and is of potential usefulness for interpretation of Auger electron angular distribution data for solid samples.[1−13] The electron is treated as a deBroglie wave-particle,[50] and each scattering atom is given a finite representation[51−54] instead of the jellium and point-charge approximations. That is, the present description allows for the inhomogeneity of electron scattering, in keeping with the behavior observed recently for ordered solid samples. Assigning a finite scattering radius to each atom maintains consistency among all components of the calculation, leads to agreement with the solid state experiments noted above, requires relatively few parameters, and is consistent with first principles.[55−57] The diffraction component of this description is a straightforward application of well-known optical modeling concepts developed by Michelson, Huygens, Fresnel, Fraunhofer, and others,[56] while the diffuse elastic component is consistent with equations presented by Mott and Massey[55] and McDaniel *et al*.[57] This empirical description of electron-scattering distributions was developed for use in converting electron scattering data to surface structure, and we hope that it will be also useful to those engaged in developing *a priori* theoretical descriptions of electron scattering.

Scattering Description

The present discussion is directed primarily toward gaseous samples with particular attention to elastic scattering. An analogous description of electron−atom scattering in solid samples will be presented in a future article. Of course, in order to arrive at an accurate and general description of observed electron scattering behavior in the solid state, it is essential to reproduce both the elastic and the inelastic scattering components.

1. Elastic Scattering. The measured elastic angular differential cross section, $q(\theta,\phi)$[19−44,55,57] is the sum of contributions due to diffuse elastic scattering f_E, diffraction f_D, and inelastic scattering,[49] f_I:

$$q(\theta,\phi) = f_E + f_D + f_I \tag{1}$$

where (θ,ϕ) is the direction of detection.

* Author to whom correspondence should be addressed.

[⊗] Abstract published in *Advance ACS Abstracts,* January 1, 1997.

S1089-5639(96)01416-8 CCC: $14.00

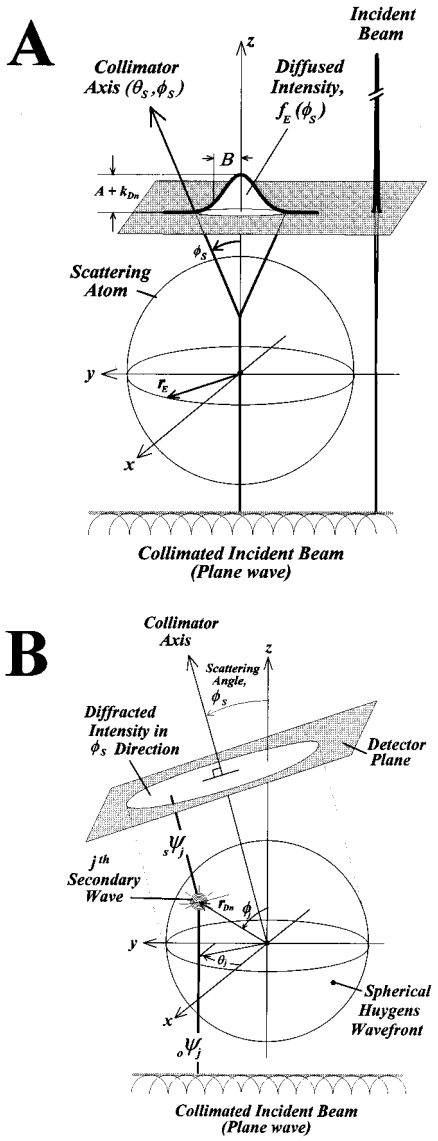

Figure 1. Schematic illustrations of the diffuse (A) and diffraction (B) portions of the electron−atom-scattering model for gaseous samples. The diffuse elastic scattering component (A) statistically disperses intensity without retention of phase information. The diffraction component of the description (B) preserves phase relationships throughout the scattering process by distributing a spherical Huygens wavefront uniformly upon the surface of the scattering atom with an effective diffraction radius, r_{Dn}. The secondary wave amplitudes are summed at the detector plane, where they interfere, producing a diffraction pattern. Summing the diffuse and diffraction components gives the observed angular variation of scattered intensity, the elastic differential scattering cross section.

a. Diffuse Elastic Scattering. Diffuse elastic scattering events are those in which the net energy transferred from the incident electron to the atom is negligible but coherent scattering is not observed, Figure 1A. Diffuse elastic scattering is thought to originate from shape resonance, core-excitation resonance, and electron-exchange and related processes, the experimental and theoretical "genealogy"[57a] of which is discussed in refs 55 and 57.

Diffuse elastic intensity is concentrated at small scattering angles and is described by the diffuse elastic scattering intensity function f_E:

$$f_E(\phi_s) = A \exp(-\phi_s/B) + C \exp[-(\pi - \phi_s)^4/D] \quad (2)$$

where ϕ_s is the polar angle of scattering; A and B describe the KE-dependent amplitude and distribution width of diffuse elastic

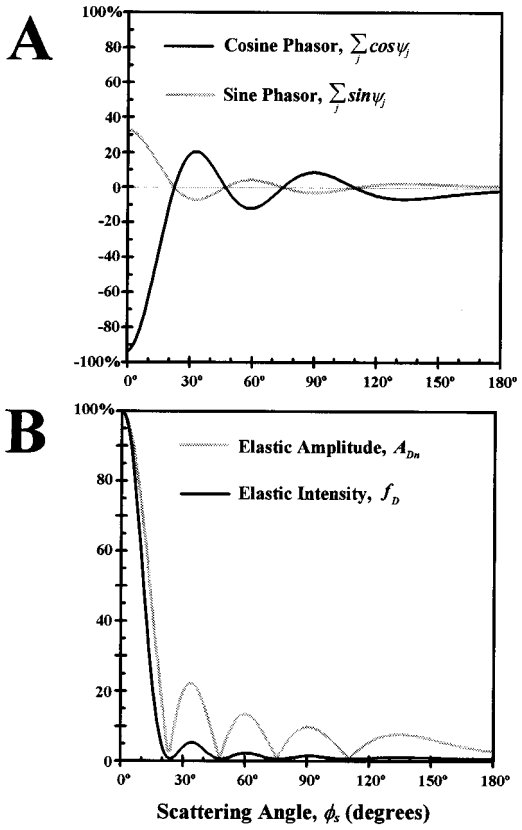

Figure 2. Graphs of diffraction functions for a single sphere of secondary waves having a radius $r_{Dn} = 1.5$ Å. (A) Elastic amplitude phase-components, or phasors, from eq 4. (B) Diffraction amplitude function A_{Dn} from eq 5 and intensity function f_D from eq 3.

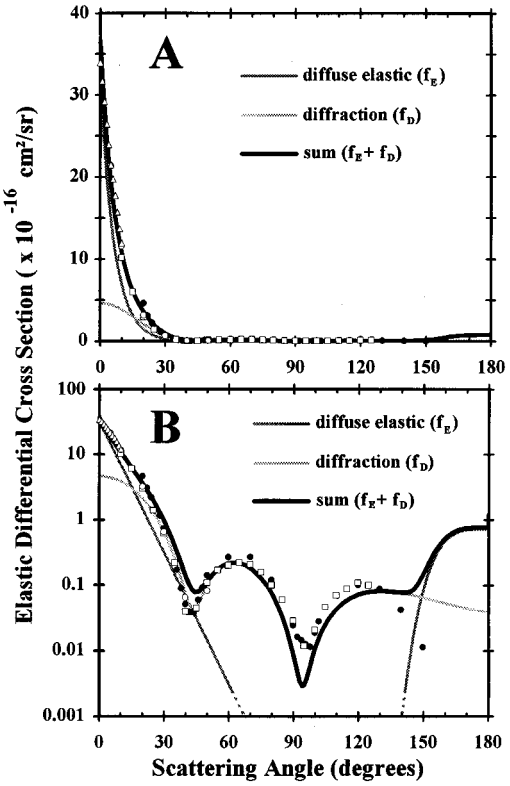

Figure 3. Elastic differential cross section data for krypton at 100 eV compared with the diffuse scattering and diffraction components of the description. Data (individual points) are from sources indicated in Figure 5. The linear display (A) illustrates that the diffuse component predominates, and its morphology differs from that of diffraction. The diffracted intensity is relatively small, but can be seen more clearly when the data are displayed on a log scale (B).

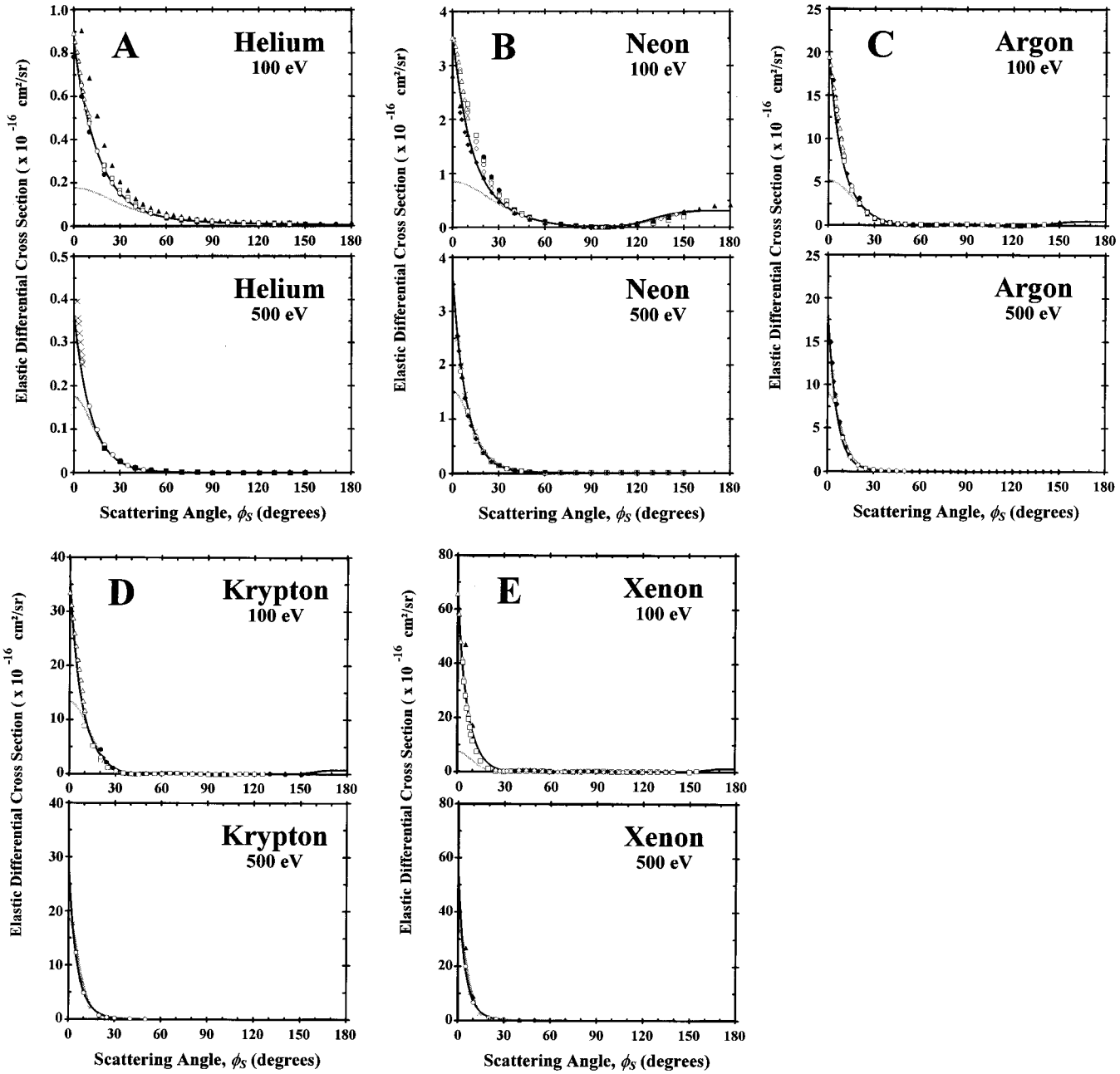

Figure 4. Linear plots of experimental differential cross section data (individual points) and the present description (heavy solid lines) for the rare gases. Note that most of the elastic scattering events result in relatively small scattering angles, especially at higher KE. (Data sources are noted in Figure 5.)

forward scattering by a specific element, respectively; and *C* and *D* describe the amplitude and distribution width of diffuse elastic backscattering, Figure 1A.

b. Diffraction. Diffraction events are those in which the phase relationships are preserved throughout the scattering process, Figure 1B. The diffraction intensity function f_D is given (according to the Born interpretation) by

$$f_D(\phi_S) = \sum_n k_{Dn} A_{Dn}^2 \tag{3}$$

where k_{Dn} is an empirical constant which describes the diffracted intensity from the nth shell. In the present work, one shell was employed to describe He ($n = 1$), while two shells (a "core shell" and a "valence shell") were used for Ne, Ar, Kr, and Xe ($n = 1$ and 2). The phase amplitude of the diffracted electron wave in a specific direction of scattering A_{Dn} is represented as the sum of all secondary waves on the Huygens wave front:

$$A_{Dn}(\phi_S) = \frac{1}{N_W}\sum_j e^{i\psi_j} = \frac{1}{N_W}\sqrt{(\sum_j \cos\psi_j)^2 + (\sum_j \sin\psi_j)^2} \tag{4}$$

where ϕ_S is the polar angle of detection, ψ_j is the final detected phase distance for the jth secondary wave, and N_W normalizes the sum by the total number of secondary waves used to compute the spherical deBroglie wavefront. The summations in eq 4 define the amplitude integral over the wavefront, and the integral can be written in closed form:

$$A_{Dn}(\theta_s,\phi_s) = \left|\frac{\sin\left\{\frac{4r_{Dn}\phi_s}{\lambda}\left[1+\frac{\sqrt{3}}{3}\cos(\phi_s/2)\right]\right\}}{\frac{4r_{Dn}\phi_s}{\lambda}\left[1+\frac{\sqrt{3}}{3}\cos(\phi_s/2)\right]}\right| = \mathrm{sinc}\left\{\frac{4r_{Dn}\phi_s}{\lambda}\left[1+\frac{\sqrt{3}}{3}\cos(\phi_s/2)\right]\right\} \tag{5}$$

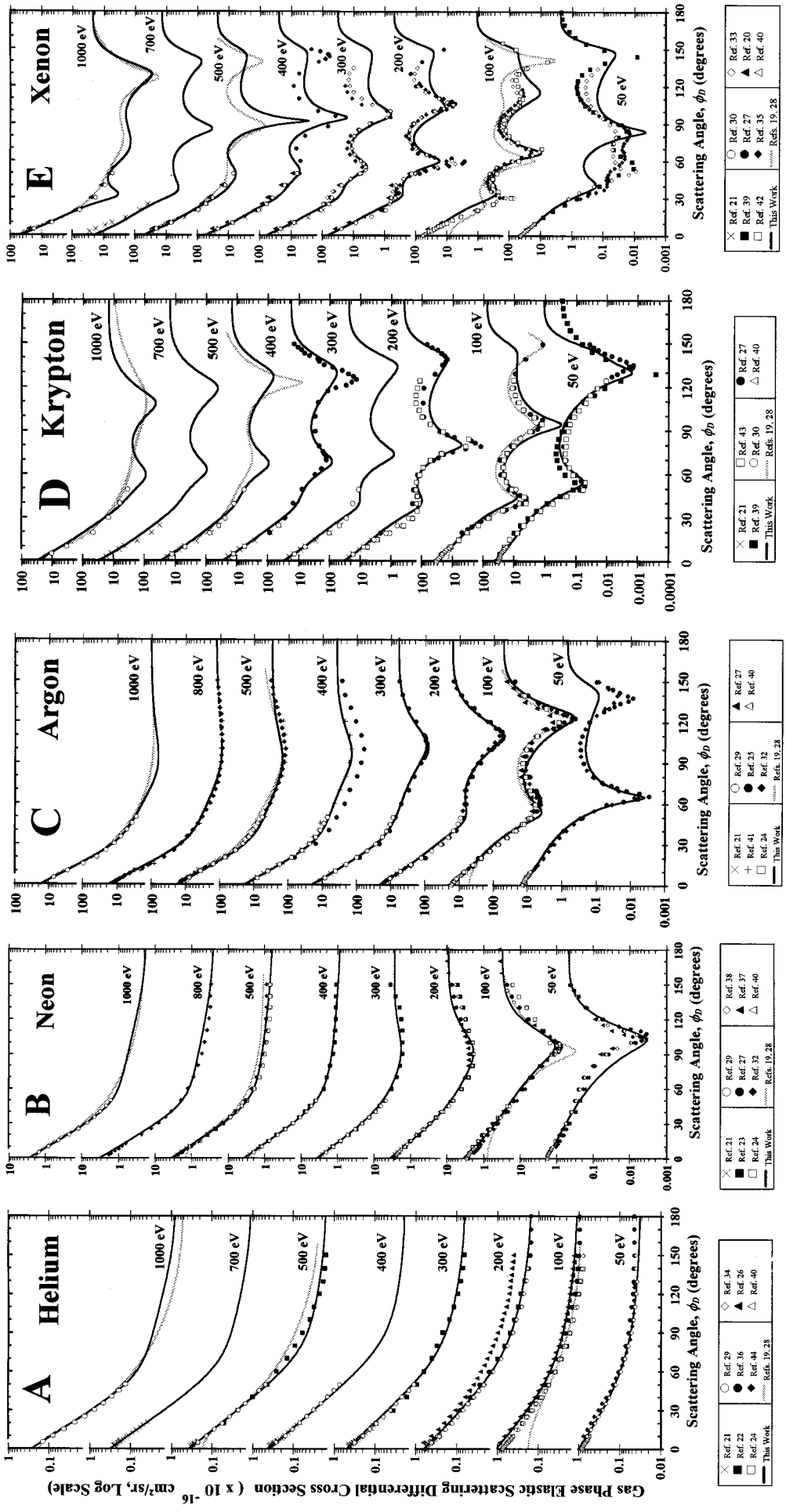

Figure 5. Logarithmic plots of experimental elastic differential cross sections for the rare gases. Gas phase measurements (individual points) are compared with the present description (heavy solid lines) and previous theoretical treatments (fine lines). References are shown in the legend below each plot. The logarithmic format allows the large-angle portions of the distributions to be seen more clearly by exaggerating the low intensities.

TABLE 1: Electron-Atom Scattering Parameters[a]

KE, eV	50	100	200	300	400	500	700	800	1000
					Helium				
A	0.97	0.82	0.65	0.52	0.416	0.365	0.32	0.305	0.269
B	20	16	14	12.71	11.73	10.93	9.78	9.4	8.7
C	0	0	0	0	0	0	0	0	0
D	1000	1000	1000	1000	1000	1000	1000	1000	1000
k_{D1}	0.06	0.028	0.008	0.003	0.0007	0.0007	0.0007	0.0007	0.0007
r_{D1}	0.18	0.17	0.14	0.11	0.09	0.084	0.0773	0.075	0.069
k_{D2}	0	0	0	0	0	0	0	0	0
r_{D2}	0	0	0	0	0	0	0	0	0
					Neon				
A	1.5	3.29	3.69	3.75	3.7	3.6	3.34	3.16	2.8
B	16	11.9	10.6	9.9	9.4	8.9	8.4	8.2	8
C	0.45	0.3	0.085	0.022	0.003	0.0013	0.0007	0.00062	0.00023
D	5.8	10	18.8	30.2	46.8	74.1	186	295	692
k_{D1}	0.5	0.32	0.05	0.02	0	0	0	0	0
r_{D1}	0.55	0.383	0.267	0.21	0.173	0.152	0.13	0.126	0.12
k_{D2}	0	0.02	0.04	0.035	0.028	0.022	0.0151	0.0142	0.014
r_{D2}	0.27	0.23	0.16	0.122	0.096	0.084	0.0773	0.075	0.069
					Argon				
A	11	18	21	20.2	19.2	18.6	18	17.5	17
B	8.2	7.3	6.58	6.3	6.08	5.87	5.64	5.6	5.6
C	0.7	0.5	0.15	0.06	0.042	0.03	0.015	0.011	0.007
D	0.6	1.66	5	12	25.7	42.7	117	182	500
k_{D1}	4.5	2.5	0.8	0.04	0.02	0	0	0	0
r_{D1}	0.81	0.69	0.53	0.45	0.404	0.38	0.34	0.32	0.293
k_{D2}	0	0.05	0.111	0.13	0.13	0.10	0.0916	0.082	0.0773
r_{D2}	0.329	0.28	0.22	0.184	0.16	0.147	0.135	0.132	0.13
					Krypton				
A	30	32	29	27	27	27	27	27	27
B	7.8	6.48	5.8	5.54	5.36	5.2	5	5	5
C	1	0.721	0.365	0.225	0.169	0.14	0.14	0.14	0.14
D	0.3	0.38	0.56	0.8	1.1	1.6	2.8	3.6	6
k_{D1}	7	4.5	2.7	1.7	1	0.81	0.6	0.52	0.4
r_{D1}	0.96	0.84	0.67	0.58	0.52	0.47	0.41	0.39	0.36
k_{D2}	0.1	0.156	0.273	0.39	0.5	0.543	0.5	0.466	0.4
r_{D2}	0.55	0.49	0.393	0.345	0.307	0.28	0.249	0.24	0.224
					Xenon				
A	39	60	65	61.3	55.4	52	49	49	49
B	6	5.3	4.58	4.27	4.13	4.09	4	4	3.96
C	2.4	1.1	0.5	0.3	0.237	0.22	0.22	0.22	0.22
D	0.2	0.2	0.222	0.249	0.296	0.36	0.542	0.684	1
k_{D1}	8.44	6.5	4.5	3.2	2.27	1.8	1.15	0.99	0.9
r_{D1}	1.3	1.11	0.85	0.73	0.64	0.58	0.489	0.453	0.41
k_{D2}	0.4	0.6	0.96	1.51	1.88	1.97	1.88	1.69	1.2
r_{D2}	0.73	0.64	0.5	0.45	0.41	0.38	0.351	0.343	0.33

[a] Units of the above quantities are for *A*, *C*, k_{D1}, and k_{D2}, cm^2/sr; *B*, degrees; *D*, (degrees)^4 × 10^6; and r_{D1} and r_{D2}, Å. The quantum mechanical radii[53,54] of He, Ne, Ar, K, and Xe are 0.31, 0.71, 0.98, 1.12, and 1.31 Å, respectively. van der Waals radii: 0.93, 1.12, 1.54, 1.69 and 1.90 Å.

where r_{Dn} is the radius of the sphere of secondary waves. The expression $|(\sin x)/x|$ in eq 5 arises frequently in optics and is denoted "sinc *x*".[61] The wavelength of the electron is given by de deBroglie relationship:

$$\lambda(\text{Å}) = \frac{h}{m_e v} = \frac{h}{(2m_e \text{KE})^{1/2}} = \left[\frac{150.4}{\text{KE(eV)}}\right]^{1/2} \quad (6)$$

where *h* is the Planck constant, m_e is the electron mass, and v is the electron velocity. The phase distance from the plane of incidence to the spherical scatterer is

$${}_o\psi_j = \frac{2\pi}{\lambda}(1 + \cos\phi_I) r_{Dn} \quad (7)$$

where (θ_j,ϕ_j) in Figure 1B is the location of the *j*th secondary wave origin on the spherical wave front. The phase distance from the origin of each secondary wave to the detector plane is

$${}_s\psi_j = \frac{2\pi r_{Dn}}{\lambda}(1 - \cos\theta_j \cos\phi_s - \cos\theta_j \sin\phi_j \sin\phi_s) \quad (8)$$

The final, detected phase is

$$\psi_j = {}_o\psi_j + {}_s\psi_j \quad (9)$$

Graphs of the diffraction phasors, $\sum_j \cos\psi_j$ and $\sum_j \sin\psi_j$, the diffracted amplitude A_{Dn}, and the diffracted intensity f_D are shown in Figure 2. The algorithm represented by eqs 3−9 is the electron scattering analog of the Huygens−Fresnel principle.[59−60]

c. Summation of Diffuse Elastic Scattering and Diffraction. The summation of diffuse elastic scattering and diffraction as described in eq 1 gives the observable elastic differential cross section, Figure 3A. The diffracted intensity f_D is relatively small, but can be seen when the data are displayed on a logarithmic scale, Figure 3B. In diffusion, f_E accounts for most of the elastic scattering, Figures 4 and 5. The morphology of diffuse elastic scattering is qualitatively different from that of diffraction, Figure 3. Although f_D and f_E are depicted separately to facilitate visualization, this does not imply that diffraction and diffuse elastic scattering are separable *a priori*.

2. Inelastic Scattering. Inelastic scattering here denotes those scattering events in which energy transfer is sufficiently large that the scattered electron is excluded by the energy filter of the detection system. Inelastic scattering affects the final observed elastic amplitude by attenuation and is the most prominent mode of scattering. Measurements of the total electron scattering cross sections of rare gas atoms reported by various laboratories[45−49] reveal a substantial KE dependence. For example, Figure 6 summarizes the values reported for Xe.[45−49] Note that inelastic processes (such as electronic excitation and ionization) constitute 70−88% of the total cross section of Xe in the 50−1000 eV KE range. Therefore, an accurate representation of the KE dependence of the total inelastic and elastic cross sections is essential to a quantitative description of electron-atom scattering. Fundamental discus-

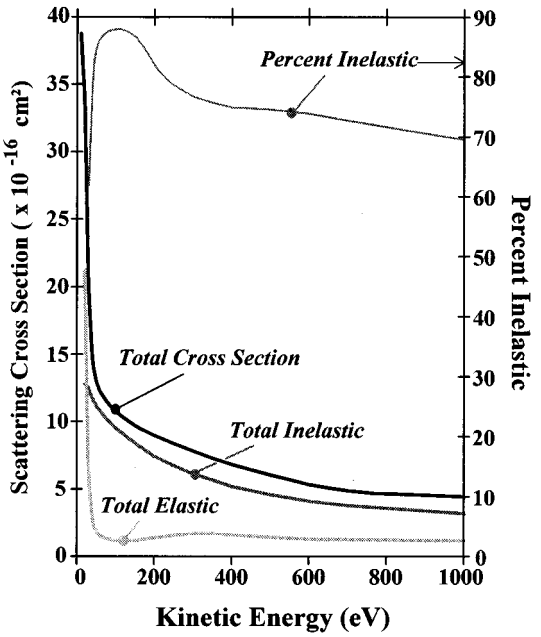

Figure 6. Experimental total electron−atom-scattering cross sections for xenon in the 0 to 1000 eV kinetic energy range.[45−49] As can be seen, electron−Xe scattering is dominated by inelastic processes at KE above ~30 eV.

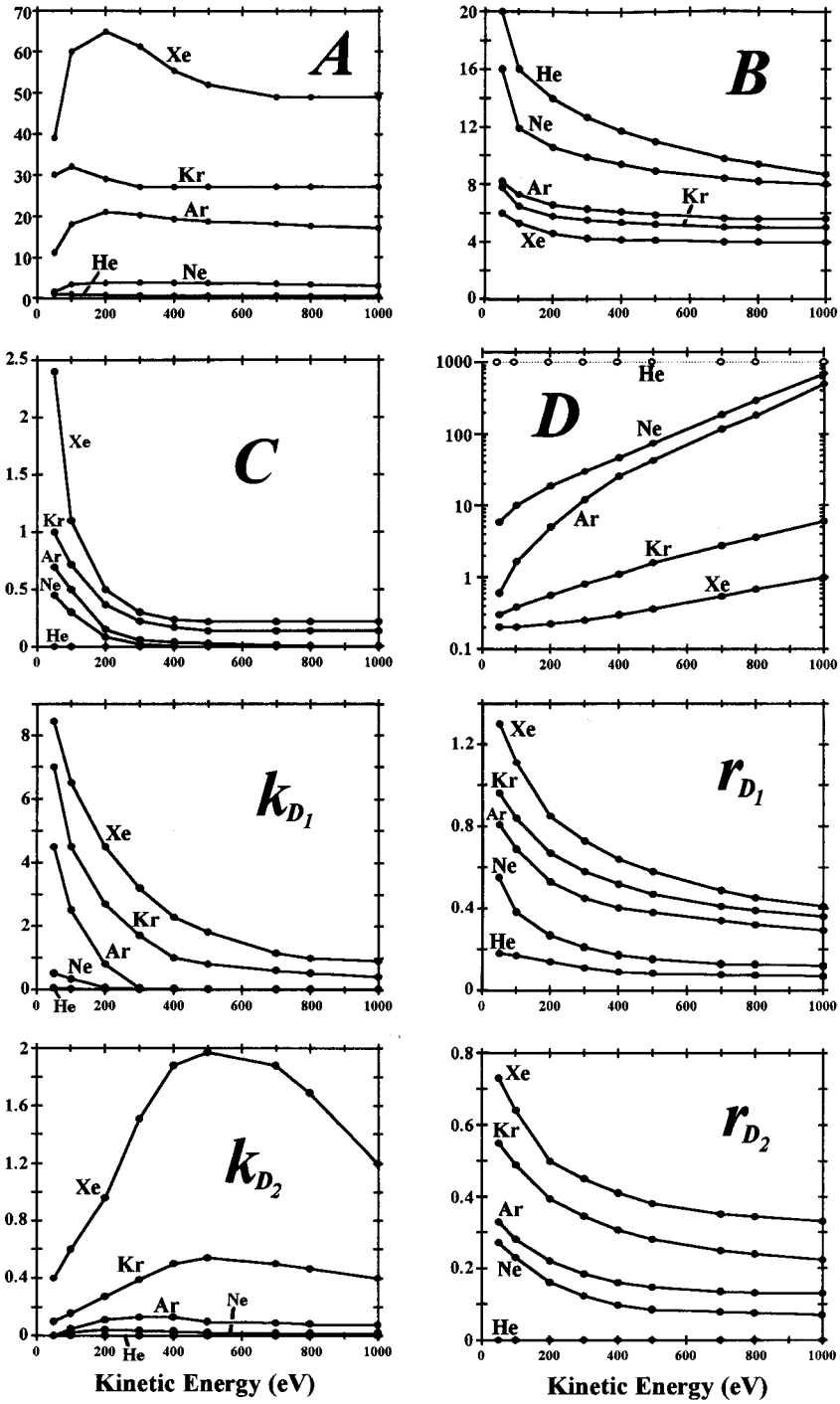

Figure 7. Graphs of model electron−atom-scattering parameters: *A*, the elastic forward scattering amplitude parameter, *B*, the elastic forward scattering distribution width parameter, *C*, the elastic backscattering amplitude parameter; *D*, the elastic backscattering distribution width parameter; k_{Dn}, the diffraction amplitude parameter; and r_{Dn}, the effective diffraction radius. Open circles indicate instances in which the contribution due to a particular component, such as backscattering by He, is vanishingly small and thus the corresponding parametric values (such as those of *D*) are indeterminate.

sions of this point are given in refs 55 and 61. In the present work, the inelastic scattering function was not allowed to vary ($f_I = 0$). The important role played by inelastic scattering in angular distributions from ordered solid samples[1−13] will be discussed in a future paper.

Comparison of the Scattering Description with Gas-Phase Data

Experimental measurements of the elastically scattered intensity which results when a collimated beam of electrons impinges upon a gaseous sample of He, Ne, Ar, Kr, or Xe are shown in Figures 4 and 5 (individual points). Specifically, the figures show the distribution of scattered intensity vs scattering angle, the "elastic differential cross section," $q(\phi_S)$, for typical electron kinetic energies. The data are graphed as originally reported, except for conversion to common units (cm^2/sr). The heavy solid lines depict elastic scattering differential cross sections calculated using the scattering model presented here. The shaded lines in Figures 4 and 5 are graphs of model calculations previously tabulated by other workers, as identified in their captions.

As can be seen from the figures, the degree of agreement between the experimental elastic differential cross sections and the model calculations is encouraging. The data clearly show that the elastically scattered intensity is concentrated at small scattering angles (the "forward direction", $\phi_S < 25°$), and the

diffraction features represent only a small fraction of the total intensity. That is, small-angle diffuse elastic scattering predominates, although diffraction effects can be seen more clearly when the data are shown on a logarithmic scale, Figure 5.

Scattering parameters for the rare gases as a function of target atomic number (Z) are listed in Table 1 and graphed in Figure 7. The parametric quantities employed in the calculations vary smoothly with KE and Z. Some useful trends are seen: The elastic forward scattering intensity parameter (A) increases with increasing Z (for elements within the same periodic group) and A increases with KE to a maximum at about 200 eV, after which it declines steadily. Elastic scattering is concentrated at the smaller scattering angles with increasing KE and Z, as seen in the elastic forward scattering distribution width parameter B. The diffraction amplitude parameter k_{Dn} and the diffraction radius parameter r_{Dn} both increase with increasing Z and decrease with increasing KE. The trends in r_{Dn} mirror those observed for other types of "atomic" radii, including van der Waals and quantum mechanical radii,[53,54] Table 1.

Summary and Conclusions

A description of electron−atom scattering has been presented which accurately reproduces observed elastic differential scattering cross sections for the rare gases.

This description combines conventional optical modeling approaches[56] with recent theoretical developments in the understanding of electron behavior.[50] Looking toward future applications of the model to crystalline solid samples, monolayers, and thin-films, scattering atoms were given finite radii, thus allowing the geometry of the scattering process to affect the calculated distribution. In particular, the point-charge and jellium approximations were not invoked.[51] The model allows for the effects of inhomogeneous electron scattering, as required for analysis of Auger electron emission angular distributions from ordered solid surfaces.[1−13] The computations are straightforward and are readily implemented with a personal computer.

The elastic scattering processes were deconvoluted from the other processes by taking advantage of the absence of geometric structure in gas-phase electron−atom-scattering experiments. The elastic portion of the description was tested in the 50−1000 eV KE range using published electron-scattering data for the rare gases.[19−49] Excellent agreement with experiment is found. Relatively few parameters are required and each parameter represents a specific property of electron scattering. The numerical values of the parameters vary smoothly with KE and Z. Accordingly, the description has potential usefulness for analysis of electron scattering behavior at surfaces and for probing surface structure and composition.

Acknowledgment. This work is supported by the National Science Foundation.

References and Notes

(1) Frank, D. G.; Batina, N.; McCargar, J. W.; Hubbard, A. T. *Langmuir* **1989**, *5*, 1141.

(2) Frank, D. G.; Batina, N.; Golden, T.; Lu, F.; Hubbard, A. T. *Science* **1990**, *247*, 182.

(3) Frank, D. G.; Lu, F.; Golden, T.; Hubbard, A. T. *MRS Bull.* **1990**, *15*, 19.

(4) Hubbard, A. T.; Frank, D. G.; Chyan, O. M. R.; Golden, T. *J. Vac. Sci. Technol.* **1990**, *B8*, 1329.

(5) Frank, D. G.; Golden, T.; Hubbard, A. T. *Science* **1990**, *248*, 1131.

(6) Frank, D. G.; Hubbard, A. T. *Langmuir* **1990**, *6*, 1430.

(7) Batina, N.; Chyan, O. M. R.; Frank, D. G.; Golden, T.; Hubbard, A. T. *Naturwissenschaften* **1990**, *77*, 557.

(8) Frank, D. G.; Golden, T.; Chyan, O. M. R.; Hubbard, A. T. *Appl. Surf. Sci.* **1991**, *48/49*, 166.

(9) Frank, D. G.; Golden, T.; Chyan, O. M. R.; Hubbard, A. T. *J. Vac. Sci. Technol.* **1991**, *A9*, 1254.

(10) Frank, D. G.; Chyan, O. M. R.; Golden, T.; Hubbard, A. T. *J. Vac. Sci. Technol.* **1992**, *A10*, 158.

(11) Frank, D. G.; Chyan, O. M. R.; Golden, T.; Hubbard, A. T. *J. Phys. Chem.* **1993**, *97*, 3829.

(12) Doyle, C. A.; Chyan, O. M. R.; Frank, D. G.; Hubbard, A. T. *Surf. Interface Anal.* **1994**, *21*, 123.

(13) Frank, D. G.; Chyan, O. M. R.; Golden, T.; Hubbard, A. T. *J. Phys. Chem.* **1994**, *98*, 1895.

(14) Felter, T. E.; Hubbard, A. T. *J. Electroanal. Chem.* **1979**, *100*, 473.

(15) Schardt, B. C.; Yau, S. L.; Rinaldi, F. *Science* **1989**, *243*, 1050.

(16) Yau, S. L.; Vitus, C. M.; Schardt, B. C. *J. Am. Chem. Soc.* **1990**, *112*, 3677.

(17) Chang, S. C.; Yau, S. L.; Schardt, B. C.; Weaver, M. J. *J. Phys. Chem.* **1991**, *95*, 4787.

(18) Hubbard, A. T. *Chem. Rev.* **1988**, *88*, 633.

(19) Fink, M.; Yates, A. C. *At. Data* **1969**, *1*, 385.

(20) Jost, K.; Fink, M.; Herrmann, D. *Abstracts*. Proceedings of the 8th International Conference on Physics of Electronic and Atomic Collisions, Belgrade, 1973; Institute of Physics: New York, 1973; p 277.

(21) Bromberg, J. P. *J. Chem. Phys.* **1974**, *61*, 963.

(22) Sethuraman, S. K.; Rees, J. A.; Gibson, J. R. *J. Phys.* **1974**, *B7*, 1741.

(23) Gupta, S. C.; Rees, J. A. *J. Phys.* **1975**, *B8*, 417.

(24) Gupta, S. C.; Rees, J. A. *J. Phys.* **1975**, *B8*, 1267.

(25) Williams, J. F.; Willis, B. A. *J. Phys.* **1975**, *B8*, 1670.

(26) Kurepa, M. V.; Vuskovic, L. *J. Phys.* **1975**, *B8*, 2067.

(27) Williams, J. F.; Crowe, A. *J. Phys.* **1975**, *B8*, 2233.

(28) Riley, M. E.; MacCallum, C. J.; Biggs, F. *At. Data Nucl. Data Tables* **1975**, *15*, 443.

(29) Jansen, R. H. J.; de Heer, F. J.; Luken, H. J.; van Wingerden, B.; Blaauw, H. J. *J. Phys.* **1976**, *B9*, 185.

(30) Jansen, R. H. J.; de Heer, F. J. *J. Phys.* **1976**, *B9*, 213.

(31) Vuskovic, L.; Kurepa, M. V. *J. Phys.* **1976**, *B9*, 837.

(32) Dubois, R. D.; Rudd, M. E. *J. Phys.* **1976**, *B9*, 2657.

(33) Buckman, S. J.; Teubner, P. J. O.; Arriola, H. *Report FIAS-R-33*; Institute for Atomic Studies, The Flinders University of South Australia, 1978.

(34) Register, D. F.; Trajmar, S.; Srivastava, S. K. *Phys. Rev.* **1980**, *A21*, 1134.

(35) Klewer, M.; Beerlage, M. J. M.; van der Wiel, M. J. J. *Phys.* **1980**, *B13*, 571.

(36) Fon, W. C.; Berrington, K. A.; Hibbert, A. *J. Phys.* **1981**, *B14*, 307.

(37) Fon, W. C.; Berrington, K. A. *J. Phys.* **1981**, *B14*, 323.

(38) Register, D. F.; Trajmar, S. *Phys. Rev.* **1984**, *A29*, 1785.

(39) McEachran, R. P.; Stauffer, A. D. *J. Phys.* **1984**, *B17*, 2507.

(40) Wagenaar, R. W.; de Boer, A.; van Tubergen, T.; Los, J.; de Heer, F. J. *J. Phys.* **1986**, *B19*, 3121.

(41) Iga, I.; Lee, M.-T.; Noguiera, J. C.; Barbieri, R. S. *J. Phys.* **1987**, *B20*, 1095.

(42) Hasenburg, K.; Bartschat, K.; McEachran, R. P.; Stauffer, A. D. *J. Phys.* **1987**, *B20*, 5165.

(43) Danjo, A. *J. Phys.* **1988**, *B21*, 3759.

(44) Brunger, M. J.; Buckman, S. J.; Allen, L. J.; McCarthy, I. E.; Ratnavelu, K. *J. Phys.* **1992**, *B25*, 1823.

(45) For total electron-atom scattering cross sections, see: (a) Dalba, G.; Fornasini, P.; Lazzizzera, I.; Ranieri, G.; Zecca, A. *J. Phys.* **1979**, *B12*, 3787. (b) Nickel, J. C.; Imre, K.; Register, D. F.; Trajmar, S.; *J. Phys.* **1985**, *B18*, 125. (c) Wagenaar, R. W.; de Heer, F. J. *J. Phys.* **1980**, *B13*, 3855. (d) Wagenaar, R. W.; de Heer, F. J. *J. Phys.* **1985**, *B18*, 2021. (e) Zecca, A.; Oss, S.; Karwasz, G.; Grisenti, R.; Brusa, R. S. *J. Phys.* **1987**, *B20*, 5157. (f) Zecca, A.; Karwasz, G.; Brusa, R. S.; Grisenti, R. *J. Phys.* **1991**, *B24*, 2737.

(46) For total electron-atom ionization cross sections, see: Krishnakumar, E.; Srivastava, S. K. *J. Phys.* **1988**, *B21*, 1055.

(47) For electron-atom excitation cross sections, see: Hayashi, M. *J. Phys.* **1983**, *D16*, 581.

(48) For electron-atom momentum transfer cross sections, see: Hayashi, M. *J. Phys.* **1983**, *D16*, 581.

(49) Total inelastic cross sections may be obtained by summing the ionization, excitation, and momentum transfer cross sections, although quantitative values for each element are not always available. In addition, cross sections obtained from various sources can vary as much as 10%.

(50) See, for example: MacGregor, M. H. *Lett. Nuovo Cimento Ital. Fis.* **1985**, *44*, 697; *Found. Phys. Lett.* **1988**, *1*, 25. deBroglie, L. In *Fifty Years of Electron Diffraction*; Goodman, P., Ed.; Reidel Pubishing Co.: Boston, 1981.

(51) The use of an "inelastic mean-free path" in scattering calculations (the "jellium model") where the structure is not random, while common, is not justified in terms of first principles. Rather, this assumption is employed for the sake of convenience, as discussed by Slater: "A complete treatment of the inelastic damping of excited electron waves [the effect of "inelastic impacts" on electron diffraction in solids], would be very complicated. In the present paper, we shall be content with a simpler task. We shall show

that an empirical damping constant can be introduced, and that solutions of the wave mechanical problem including this damping give exponentially damped waves, of the sort to be expected intuitively". Slater, J. C. *Phys. Rev.* **1937**, *51*, 840.

(52) Greenwood, N. N.; Earnshaw, A. *Chemistry of the Elements*; Pergamon Press: Oxford, 1984.

(53) Pauling, L. The Nature of the Chemical Bond; Cornell University Press: Ithaca, New York, 1960.

(54) *Lange's* Handbook of Chemistry, 13th ed.; Dean, J. A., Ed.; McGraw Hill: New York, 1985.

(55) The commonly accepted underpinning of rigorous discussions of electron scattering is the "overlap" of the wavefunction of the propagating electron with the wave functions of the ground and excited states of the scattering centers (atoms or ions). See, for example: eq 16.76 and the accompanying discussion in: Mott, N. F.; Massey, H. S. W. *The Theory of Atomic Collisions*; Oxford University press: London, 1965.

(56) Hecht, E. *Optics*, 2nd ed.; Addition-Wesley: Reading, Massachusetts, 1987.

(57) (a) McDaniel, E. W. *Atomic Collisions*. *Electron and Photon Projectiles*; Wiley: New York, 1989; (b) Shimamura, I., Takayanagi, K., Eds. *Electron-Molecule Collisions*; Plenum Press: New York, 1984. (c) Schulz, G. J. *Revs. Mod. Phys.* **1973**, *45*, 378.

(58) The "visibility" of a circular source, as described by Michelson, has the functional form $|\mathrm{sinc}(x)|$, which is analogous to the continuous-spherical-emitter description given here. See ref 56 for a more complete discussion of the sinc function.

(59) Huygens' principle: "Every point on a primary wavefront serves as the source of spherical secondary wavelets, such that the primary wavefront at some later time is the envelope of these wavelets. Moreover, the wavelets advance with a speed and frequency equal to those of the primary wave at each point in space." See ref 56, p 80.

(60) The Hyugens−Fresnel principle. "Every unobstructed portion of a wavefront, at a given instant in time, serves as a source of spherical secondary wavelets. The amplitude of the optical field at any point beyond is the superposition of all these wavelets, considering their amplitudes and relative phases." See ref 56, p 392.

(61) Gryzinski, M. *Phys. Rev.* **1965**, *A138*, 305. (a) Ibid. p 322; (b) Ibid. p 336.